Supporting Information

Fe-Doped NiCoP Nanosheet Arrays Rich in Phosphorus Vacancies for Highly Efficient Electrochemical Water Splitting

Wei Chen,[a] *Wanli Tian,* [a] *and Kai Tao*[a*]

[a] School of Materials Science & Chemical Engineering, Ningbo University, Ningbo, Zhejiang 315211, China.

*Correspondence author.

E-mail: taokai@nbu.edu.cn (K. Tao).

Experimental

Materials and Chemicals

All chemicals and reagents were used as received without further purification. The chemical reagents, including cobalt(II) nitrate hexahydrate ($Co(NO_3)_2 \cdot 6H_2O$, 98%), 2-methylimidazole (2-MIM, 99%), potassium hexacyanoferrate(II) trihydrate ($K_4[Fe(CN)_6] \cdot 3H_2O$, 98%), and sodium hypophosphite (NaH_2PO_2, 98%) were purchased from Sinopharm Chemical Reagent Co., Ltd. Nickel foam (NF) was obtained from J&K Chemical Technology and pretreated with 1 M HCl (30 min immersion) followed by sequential rinsing with deionized water and ethanol. Ruthenium (IV) oxide (RuO_2), platinum-loaded carbon (Pt/C, 20 wt%), and Nafion solution (5%) were commercially acquired.

Preparation of Pt/C and IrO_2 electrodes

Commercial Pt/C or IrO_2 was dispersed into a solution containing ethanol, deionized water and Nafion. After sonication for 30 min, the resulting suspension was coated on 1 cm^2 of NF and then dried in an oven.

Characterization

The morphology and microstructure of the electrocatalysts were investigated using a scanning electron microscope (SEM, Nova Nano SEM 450) equipped with an energy dispersive X-ray spectrometer (EDS), and a transmission electron microscope (TEM, FEI Tecnai TF20). X-ray diffraction (XRD) patterns were acquired by a Bruker AXS D8 Advance X-ray diffractometer using Cu Kα radiation (λ= 1.5406 Å). X-ray photoelectron spectroscopy (XPS) measurements were performed on a Thermo

Scientific ESCA-Lab-200i-XL spectrometer. Electron paramagnetic resonance (EPR) spectra were recorded by a Bruker EPR EMXPLUS 10/12 spectrometer at 100 K temperature.

Electrochemical measurements

The electrochemical performance of the prepared electrocatalysts was evaluated by an electrochemical workstation (CHI 760E, Shanghai Chenhua Instrument Co., Ltd.). All the measurements were carried out in 1 M KOH electrolyte by assembling a three-electrode cell, in which Hg/HgO, platinum wire and as-prepared electrocatalysts acted as the reference, counter and working electrodes, respectively. The measured potentials were all converted with reference to the reversible hydrogen electrode (RHE) according the equation: E (*vs.* SHE)=E (*vs.* Hg/HgO)+ 0.059×pH+0.098 V. Tafel plots were collected from the linear part (η=a+blog$j$) of the function (η *vs.* log$j$), where b was the Tafel slope, j was the current density and a was a constant. The measurement of electrochemical impedance spectroscopy (EIS) requires first activating the catalyst through cyclic voltammetry (CV) (for example, 20 cycles) to ensure stable performance. Subsequently, the EIS test is conducted at the target reaction potential (for instance, HER close to 0 V vs RHE or OER above 1.23V vs RHE), with the frequency typically ranging from 100 kHz to 0.01 Hz and an amplitude of the sinusoidal voltage of 5 mV. Each current density measurement was repeated twice to ensure data reliability and accuracy.

Cyclic voltammetry (CV) measurements were performance at different scan rate in the non-faradaic potential range to obtain the double layer capacitance (C_{dl}). The C_{dl}

and electrochemical surface area (ECSA) were estimated by eq. (S1) and eq. (S2).

$Cdl=\Delta j/2\upsilon$ (S1)

$ECSA=Cdl/Cs$ (S2)

Which Δj is the current density difference between the anode and cathode, v is the scan rate and C_s is the specific capacitance, here use 40 mF cm^{-2}.

Bubbling method which recording data of the rising volume V (mL) of the soap bubble and the total number of charges transferred under constant current (200 mA cm^{-2}) was measured to calculate the Faraday efficiency (FE) as eq. (S1)

$FE=4 * F * V/(1000 * V_m * It)$ (S3)

Where F is the Faraday constant 96485 C mol^{-1}, V is the volume change of oxygen or hydrogen production (mL) and V_m is the molar volume (molar under normal temperature and pressure, 24.5 L mol^{-1})

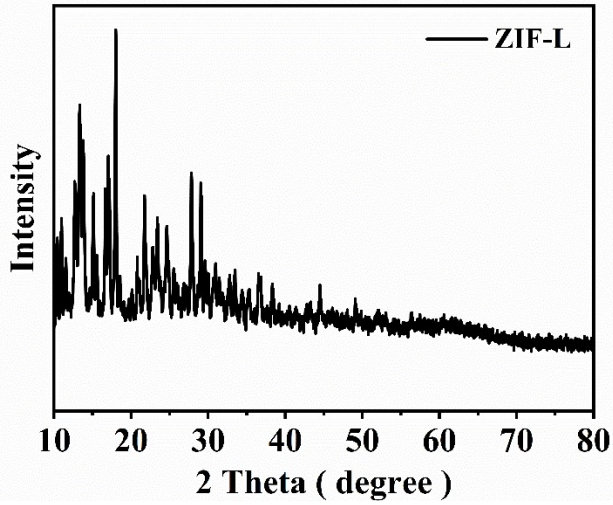

Figure S1. XRD patterns of ZIF-L

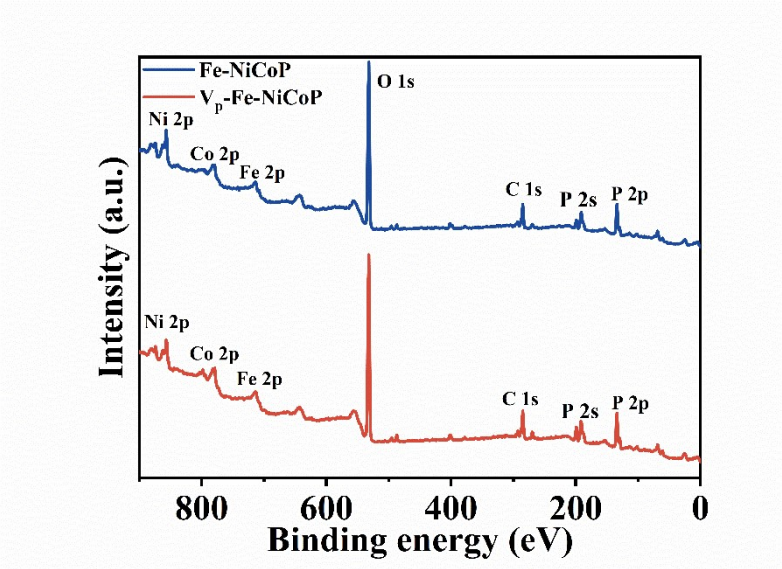

Figure S2. XPS survey spectra of Fe-NiCoP and V_p-Fe-NiCoP

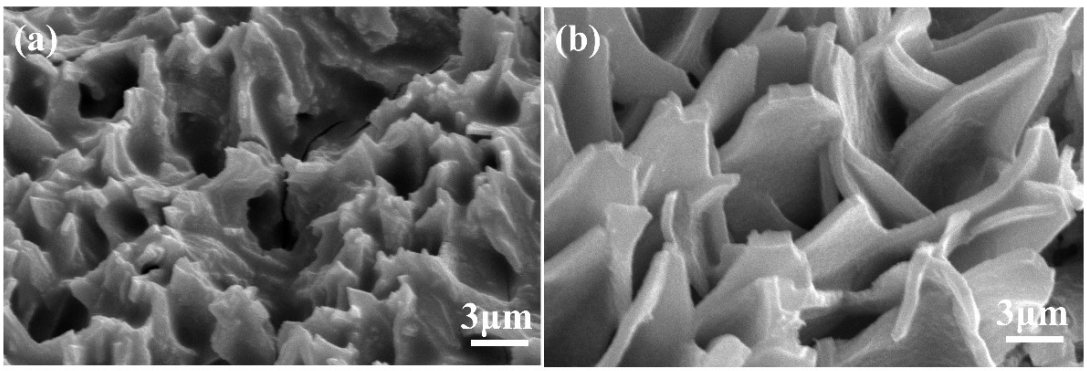

Figure S3. SEM images of (a) NF-P and (b) ZIF-L-P

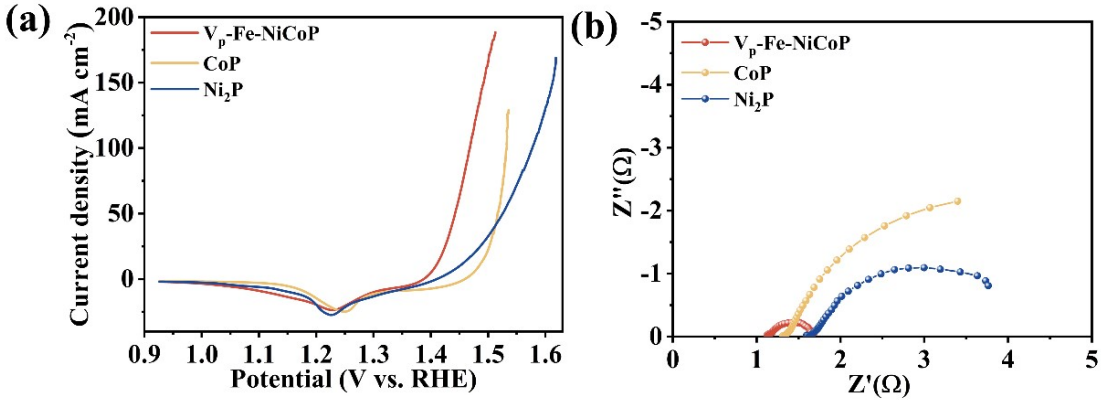

Figure S4. (a) LSV curves and (b) Nyquist plots of NF-P, ZIF-L-P and V_p-Fe-NiCoP.

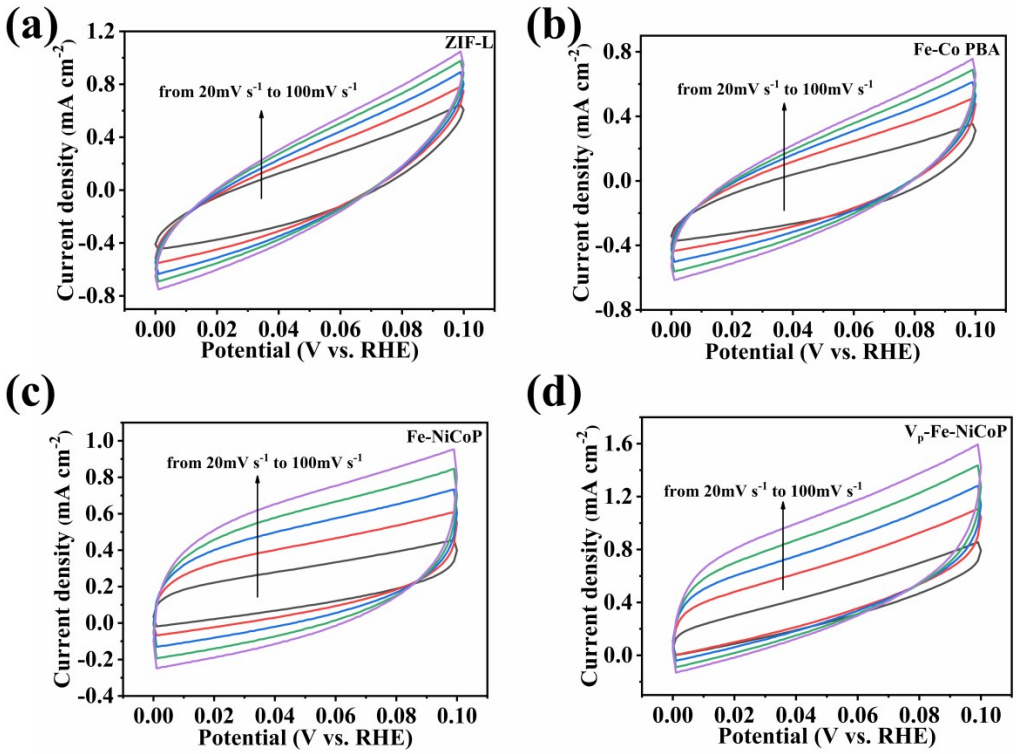

Figure S5. CV curves of (a) ZIF-L, (b) Fe-Co PBA, (c) Fe-NiCoP and (d) V_p-Fe-NiCoP collected at non-faradaic regions (0~0.1 V *vs* RHE).

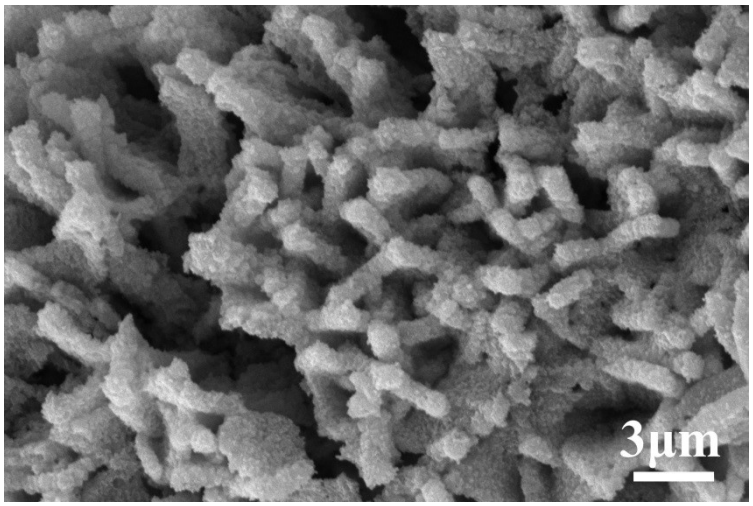

Figure S6. SEM image of the V_p-Fe-NiCoP after OER.

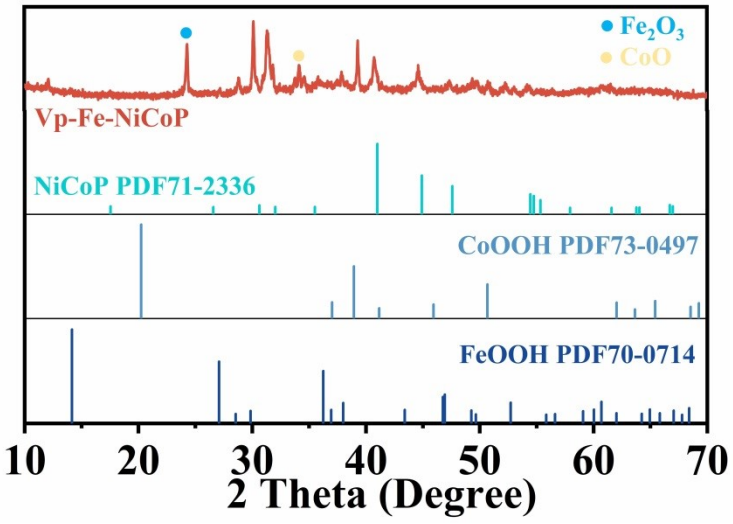

Figure S7. XRD pattern of the V_p-Fe-NiCoP after OER.

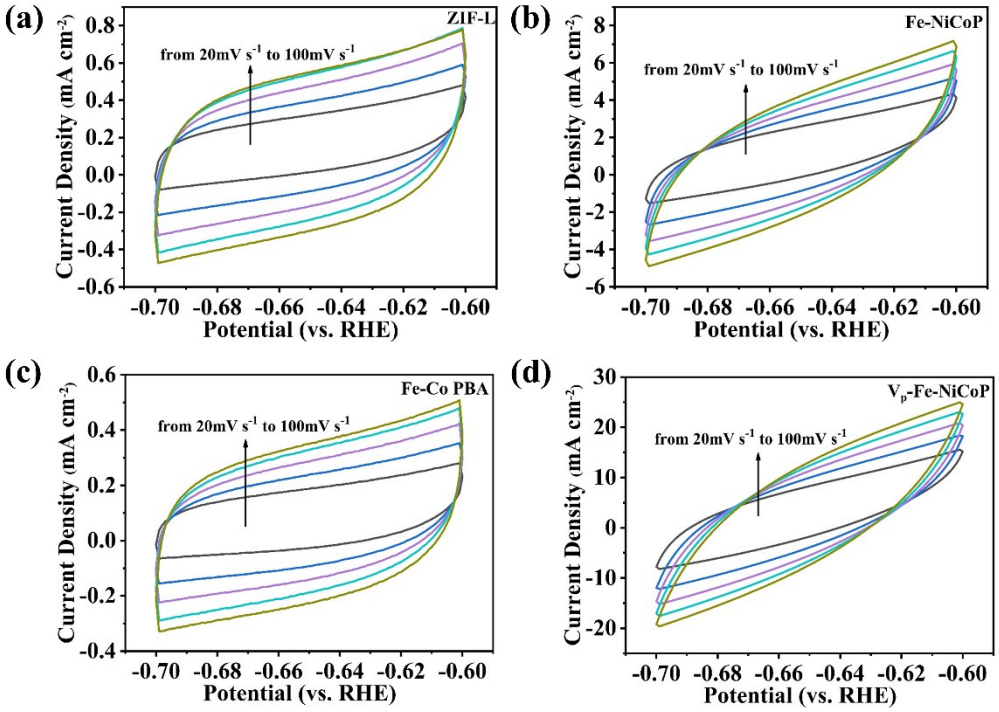

Figure S8. CV curves of (a) ZIF-L, (b) Fe-Co PBA, (c) Fe-NiCoP and (d) V_p-Fe-NiCoP collected at non-faradaic regions (-0.7~-0.60 V *vs* RHE).

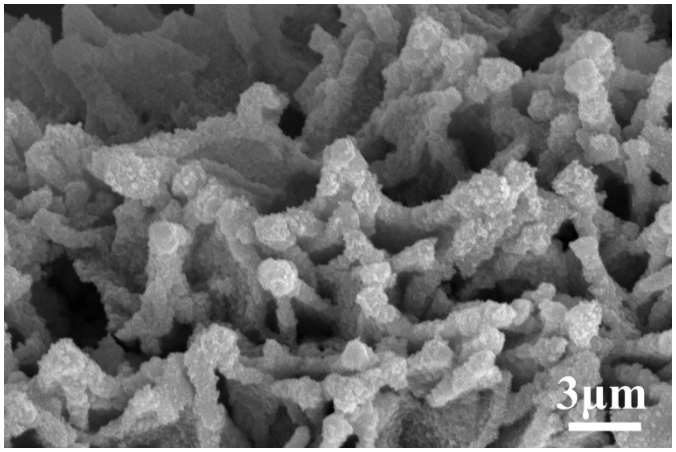

Figure S9. SEM image of the V_p-Fe-NiCoP after HER.

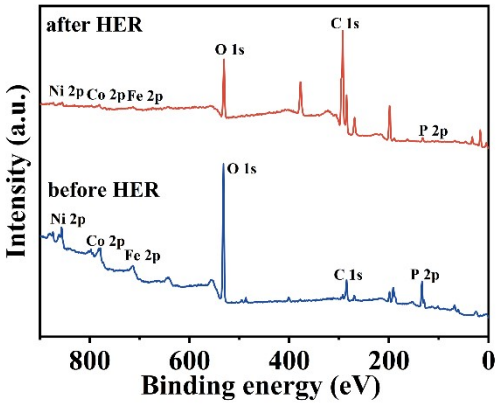

Figure S10. XPS spectra of V_p-NiCoP after HER.

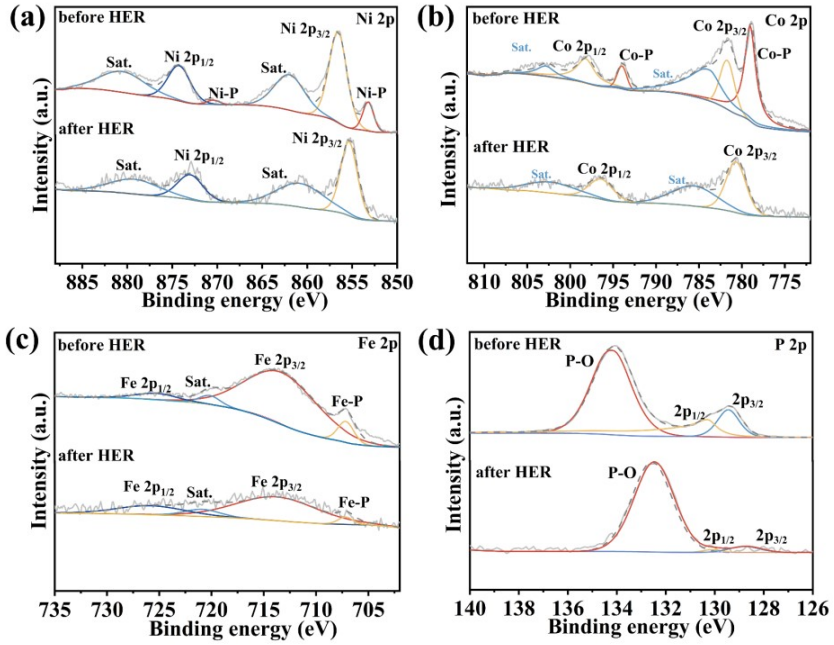

Figure S11. XPS spectra of V_p-NiCoP before and after HER. (a) Ni 2p, (b) Co 2p, (c) Fe 2p and (d) P 2p.

Table S1. Comparison of OER performances between V_p-Fe-NiCoP and other reported electrocatalysts

Electrocatalysts	Electrolyte (KOH)	*j* (mA/cm^2)	η (mV)	Tafel slope (Mv/dec)	Reference
V_p-Fe-NiCoP	1M	100	240	85	This work
NiCoP	1M	10	273	88.9	S1
Fe-CoP	1M	10	269	96.37	S2
CeO_2-$NiCoP_x$	1M	10	260	72	S3
Ni-CoP_3	1M	100	306	154	S4
FeCoNi-P	1M	100	303.9	55.87	S5
P_v-CoP	1M	10	297	58.1	S6
Ce-NiCoP/Co_3O_4/NF	1M	100	270	63.1	S7

Table S2. Comparison of HER performances between V_p-Fe-NiCoP and other reported electrocatalysts.

Electrocatalysts	Electrolyte (KOH)	*j* (mA/cm^2)	η (mV)	Tafel slope (Mv/dec)	Reference
V_p-Fe-NiCoP	1M	-100	164	65	
NiCoP	1M	-10	134.6	72.3	S1
Fe-CoP	1M	-10	203	120	S2
Ce-NiCoP/Co_3O_4/NF	1M	-100	270	48.3	S7
Fe0.4NiCoP/C	1M	-10	107	76	S8
NiCoP-BDC-4/NF	1M	-50	170	95.3	S9

Table S3. Comparison of overall water splitting performances between V_p-Fe-NiCoP and other reported electrocatalysts

Catalyst	Electrolyte	Electrolyzer	Cell voltage (V)	Reference
V_p-Fe-NiCoP	1M KOH	Vp-Fe-NiCoP||Vp-Fe-NiCoP	1.46 (10 mA cm^{-2}) 1.7 (100 mA cm^{-2})	This work
NiCoP/NiFeP	1M KOH	NiCoP/NiFeP|| NiCoP/NiFeP	1.705 (100 mA cm^{-2})	S10
Ni_2P/CoP/FeP_4	1M KOH	Ni_2P/CoP/FeP_4|| Ni_2P/CoP/FeP_4	1.5 (10 mA cm^{-2})	S11
NiFeP/CoP	1M KOH	NiFeP/CoP|| NiFeP/CoP	1.72 (10 mA cm^{-2})	S12
Ni_2P-CoP/MoO_2	1M KOH	Ni_2P-CoP/MoO_2||NiFe LDH	1.5 (10 mA cm^{-2})	S13
CoP/FeP@NF	1M KOH	CoP/FeP@NF|| CoP/FeP@NF	1.56 (10 mA cm^{-2})	S14

References

S1 Ding, M.; Yu, Q.; Wei, Z.; Liu, D., ZIF-67-templated NiCoP bimetallic catalysts for enhanced water splitting performance. *Materials Science in Semiconductor Processing* 2025, 192, 109461.

S2 Yuan, Y.; Yang, Y.; Xie, H.; Zhong, X.; Wang, R.; Xu, Z., Trace Fe doping improved the OER and HER catalytic performance of CoP hollow nanoflower clusters. *International Journal of Hydrogen Energy* 2024, 90, 1401-1410.

S3 Wen, S.; Huang, J.; Li, T.; Chen, W.; Chen, G.; Zhang, Q.; Zhang, X.; Qian, Q.; Ostrikov, K., Multiphase nanosheet-nanowire cerium oxide and nickel-cobalt phosphide for highly-efficient electrocatalytic overall water splitting. *Applied Catalysis B: Environmental* 2022, 316,121678.

S4 Muhammad, P.; Zada, A.; Rashid, J.; Hanif, S.; Gao, Y.; Li, C.; Li, Y.; Fan, K.; Wang, Y., Defect Engineering in Nanocatalysts: From Design and Synthesis to Applications. *Advanced Functional Materials* 2024, 34 (29),2314686.

S5 Guo, Y.; Wang, P.; Li, P.; Tang, M.; Yin, H.; Wang, D., A highly efficient and durable self-standing iron-cobalt-nickel trimetallic phosphide electrode for oxygen evolution reaction. *Journal of Alloys and Compounds* **2023,** 960,170493.

S6 Yuan, G.; Bai, J.; Zhang, L.; Chen, X.; Ren, L., The effect of P vacancies on the activity of cobalt phosphide nanorods as oxygen evolution electrocatalyst in alkali. *Applied Catalysis B: Environmental* **2021,** 284,119693.

S7 Liu, Z.; Lee, S.; Zhou, T.; Yang, J.; Yu, T., Ce-doped NiCoP/ Co3O4 composite Nanostructures on Ni foam and their enhanced performance for water and urea electrolysis. *Journal of Colloid and Interface Science* **2025,** 692,137542.

S8 Wang, G.; Zhang, H.; Xiang, J., Component regulation in flower-like FexCoNiP/C nanohybrids as bifunctional efficient electrocatalysts for overall water splitting. *Electrochimica Acta* **2024,** 500,144751.

S9 Ogundipe, T. O.; Shen, L.; Shi, Y.; Lu, Z.; Wang, Z.; Tan, H.; Yan, C., Nickel-cobalt phosphide terephthalic acid nano-heterojunction as excellent bifunctional electrocatalyst for overall water splitting. *Electrochimica Acta* **2022,** 421,140484.
S10 Gan, J.-C.; Zhang, L.; Feng, J.-J.; Shi, Y.-C.; Li, X.-S.; Wang, A.-J., Self-supporting highly branched urchin-like NiCoP/NiFeP heterostructures as efficient bifunctional electrocatalyst for overall water splitting. *Journal of Colloid and Interface Science* **2025,** *687*, 24-35.
S11 Zhao, T.; Gong, B.; Xu, G.; Jiang, J.; Zhang, L., In situ surface reconstruction of heterostructure Ni2P/CoP/FeP4 nanowires network catalyst for high-current-density overall water splitting. *Chinese Journal of Catalysis* **2024,** *61*, 269-280.
S12 Li, G.-L.; Miao, Y.-Y.; Deng, F.; Wang, S.; Wang, R.-X.; Lu, W.-H.; Chen, R.-L., Highly-dispersed 2D NiFeP/CoP heterojunction trifunctional catalyst for efficient electrolysis of water and urea. *Journal of Colloid and Interface Science* **2024,** *667*, 543-552.
S13 Tan, C.; Huang, S.; Lu, L.; Dong, L.; Pang, Q.; Fan, M.; Li, B.; He, H.; Chen, Z., Hierarchical multiphase heterointerfaces Ni2P–CoP/MoO2 catalyst for efficient and stable hydrogen evolution reaction over the entire pH range. *Journal of Power Sources* **2024,** 611,234757.
S14 Guan, M.; Fu, S.; Qin, F.; Zuo, P.; Shen, W., Urchin-like bifunctional CoP/FeP electrocatalyst for overall water splitting. *International Journal of Hydrogen Energy* **2024,** 93, 147-157.